









<https://doi.org/10.1038/s43247-023-00899-y>

OPEN

Paleobathymetric reconstructions of the SW Barents Seaway and their implications for Atlantic–Arctic ocean circulation

Amando P. E. Lasabuda ^{1,2✉}, Alfred Hanssen ¹, Jan Sverre Laberg ¹, Jan Inge Faleide ³, Henry Patton ⁴, Mansour M. Abdelmalak ³, Tom Arne Rydningen ¹ & Bent Kjølhamar ⁵

Unravelling past, large-scale ocean circulation patterns is crucial for deciphering the long-term global paleoclimate. Here we apply numerical modelling to reconstruct the detailed paleobathymetry-topography of the southwestern inlet of the Barents Seaway that presently connects the Atlantic and Arctic oceans. Subaerial topography was likely enough to block Atlantic Water from entering the Barents Seaway in the earliest Eocene (c. 55 Ma). The water may have entered in the middle Eocene (c. 47 Ma) as observed from major basin subsidence, but paleotopographic highs to the east may have hindered connections between the two oceans. From the Oligocene (c. 33 Ma) until the onset of the Quaternary (c. 2.7 Ma), basin shallowing and regional shelf uplift blocked Atlantic Water from entering the Barents Seaway. Our results imply that the Fram Strait remained the sole gateway for Atlantic Water into the Arctic Ocean since its opening in the Miocene until the Quaternary.

¹Department of Geosciences, UiT The Arctic University of Norway, N-9037 Tromsø, Norway. ²Department of Earth Sciences, Royal Holloway University of London, Egham, UK. ³Department of Geosciences, University of Oslo, Oslo, Norway. ⁴CAGE—Centre for Arctic Gas Hydrate, Environment and Climate, Department of Geosciences, UiT The Arctic University of Norway, N-9037 Tromsø, Norway. ⁵TGS, Oslo, Norway. ✉email: amando.lasabuda@uit.no

Ocean gateways and seaways play a major role as conduits that connect oceans and link their circulation. While gateways are likely related to opening of an ocean due to plate separation and therefore, are formed on oceanic crust (e.g., Fram Strait Gateway, Southern Ocean Gateways), the term “seaways” can be used more loosely to describe newly formed sea connections that often form on a continental crust (e.g., Barents Seaway). Seaways are also commonly used to describe a closure of two previously connected oceans (e.g., Tethys Seaway, Central American Seaway)¹ and are generally wider and shallower than straits/gateways (e.g., Bering Strait, Nares Strait, Fig. 1a)².

Ocean circulation is particularly important for Arctic climate as heat and moisture are distributed from lower to higher latitudes by the circulation of water masses^{3,4}. At present, the North Atlantic and Arctic oceans are linked through the Fram Strait Gateway (Fig. 1a)⁵, and via the Barents Sea shelf (i.e., the Barents Seaway), which presently accounts for ~50% of the inflow of Atlantic Water into the Arctic Ocean⁶ (Fig. 1a). So far, work has largely focused on the evolution of the Fram Strait^{1,4,7–11}, and very little is presently known on the Barents Seaway and its evolution, including its configuration since the Eocene (starting at c. 55 Ma) and through the repeated glaciations of the Quaternary (c. 2.7 Ma). This knowledge gap is, at least partly, due to complexities involved in restoring glacial and pre-glacial paleobathymetry-topography on the glaciated Barents Sea margin. These complexities result from the intricate relationship of erosion–deposition (i.e., uncertainties in estimating the thickness of missing strata on the shelf and their time of erosion), the timing and effects of loading–unloading of sediments that resulted in flexural isostatic adjustment, and the complex rifting-related processes on this passive margin, see review by Lasabuda et al.¹² (Fig. 1b).

Prior to the formation of the present-day Barents Seaway, early-mid Cenozoic tectonism caused oblique extension in the study area and finally it became a sheared margin after breakup. These events created overall rifting of sedimentary basins in the SW Barents Sea and stretching of the lithosphere. These effects are suggested to be laterally variable across the continental margin (i.e., spatial variation of beta factor/stretching), due to the variability of bedrock composition in the basins and highs in this area^{13,14}. The cessation of rifting activity and cooling of the asthenosphere and the lithosphere caused thermal subsidence, the timing and effects of which must be accounted for to reconstruct the paleobathymetry-topography of the Barents Seaway area. Furthermore, unloading of sediments due to erosion by shallow marine, coastal, fluvial and glacial processes have influenced the paleobathymetry-topography of the shelf through flexural isostatic adjustment of the underlying lithosphere^{15–17} (Fig. 2a). Finally, sea-level variation throughout the Cenozoic might affect the reconstructed paleobathymetry-topography^{18,19}, although this aspect may be of minor importance if the wider Barents Seaway is considered (see below).

Structural elements of the SW Barents Sea continental shelf consist of basins, highs/ridges and platforms as a result of Palaeozoic—early Cenozoic tectonic episodes, while the present-day bathymetry is characterized by major troughs and banks, shaped by glacial activity during the Quaternary (Fig. 2a, b). The paleogeographic (i.e., paleobathymetric–topographic) evolution of the Barents Shelf has mainly been reconstructed based on geomorphologic analysis using seismic reflection profiles and lithologic information from well data. Such reconstructions include the Paleocene–Eocene period of SW Barents Sea^{14,20,21} and the broader circum-Arctic^{22,23}, whose reconstructions were possible using the relatively widespread distribution of Paleocene–Eocene sediments. However, there is still a high uncertainty in reconstructing bathymetry of the succeeding time

interval (i.e., Oligocene–Miocene) based on solely subsurface data as these sediments are spatially limited. Previous paleobathymetric reconstructions for the Eocene–Quaternary are mostly more regional and of low resolution^{1,8,15–17,24} (Table 1). Thus, a detailed, high-resolution Eocene–Quaternary paleobathymetric reconstruction is lacking for the SW Barents Sea, an important area as it today acts as a shallow-water seaway for a considerable volume of Atlantic Water to enter the Arctic Ocean that has implications for thermohaline circulation including ocean temperatures and sea-ice cover²⁵.

Prior to the early Cenozoic breakup separating Eurasian and Greenland plates, Cretaceous and earlier rifting events created deep sedimentary basins in the SW Barents Sea (e.g., Sørvestsnaget, Tromsø and Bjørnøya basins). The Cenozoic plate breakup at the Paleocene–Eocene transition (c. 55 Ma) was followed by seafloor spreading in the Norwegian–Greenland Sea. This major event affected vast areas along the western Barents Sea continental margin and resulted in a series of rotated fault blocks that affected Paleocene to mid-upper Eocene strata (Fig. 3a). This Cenozoic breakup was part of a broader Eureka deformation²⁶ involving Svalbard, NE Greenland and the Ellesmere Island in Arctic Canada.

In the Oligocene (c. 33 Ma), a major plate reorganization occurred where the Greenland plate moved northwestward together with North America. The Barents Shelf is generally considered to have been tectonically stable in this period, except locally in the Vestbakken Volcanic Province where rifting extended to the Oligocene¹³. Oligocene–Miocene strata are rather thin and restricted throughout the study area (Fig. 3a). In the Miocene, opening of the Fram Strait Gateway occurred, allowing for a ventilated Arctic Ocean (as today) from around 17 Ma^{4,10} that resulted in ocean circulation between NE Atlantic and Arctic oceans as evidenced from contourite sediment accumulations along the margins of the Barents Shelf^{27,28} and other nearby areas^{29,30}.

The Quaternary marks the onset of major shelf-wide, ice-sheet glaciations in the Eurasian Arctic, including across the Barents Sea shelf. This glacial activity was responsible for major erosion of the shelf and the accumulation of eroded sediments along the western and northern continental margins of the Barents Sea, such as the Bjørnøya Trough Mouth Fan (TMF)^{31–35}. The thickness of the Bjørnøya TMF today is up to 3.5 km, containing a total volume of up to 464,000 km³^{36–41}.

Unloading of sediments from the shelf resulted in the uplift of sedimentary basins to the extent of affecting hydrocarbon reservoir properties and leakage⁴² and hydrate-related fluid flow⁴³ (Fig. 3b). The net erosion is estimated to have varied across structural elements in Barents Shelf and temporally throughout the Cenozoic^{12,14,17,39,44–49}. In the western basins, net average glacial erosion is estimated to be 0–1500 m with differential erosion associated to troughs (c. 1000 m) and banks (c. 500 m)³⁷. For the Miocene (pre-glacial), it has been suggested that the average erosion was markedly lower, c. 250 m concentrated in the area of Hammerfest Basin and up to c. 450 m on structural highs, such as Stappen High and Loppa High (these highs were not part of the modelling presented here)¹⁴.

This study focuses on the SW Barents Sea continental margin (Fig. 2b), part of the Norwegian Arctic where Atlantic Water masses currently split in two directions: one continuing northwards along the continental slope, and the other entering shelf areas (i.e., the southern inlet of the Barents Seaway). Our approach utilizes a 3D ‘backstripping’ technique^{50,51}, which sequentially restores each sedimentary layer in a time-transgressive manner. We use the 3D MOVE numerical modelling software, in which parameters account for lithosphere thickness^{52,53}, a beta factor for crustal stretching^{54,55} as well as glacial erosion and sediment properties^{14,32,37} (Fig. 2c, d). Thus, the aims of this paper are: (i) to model the paleobathymetry-

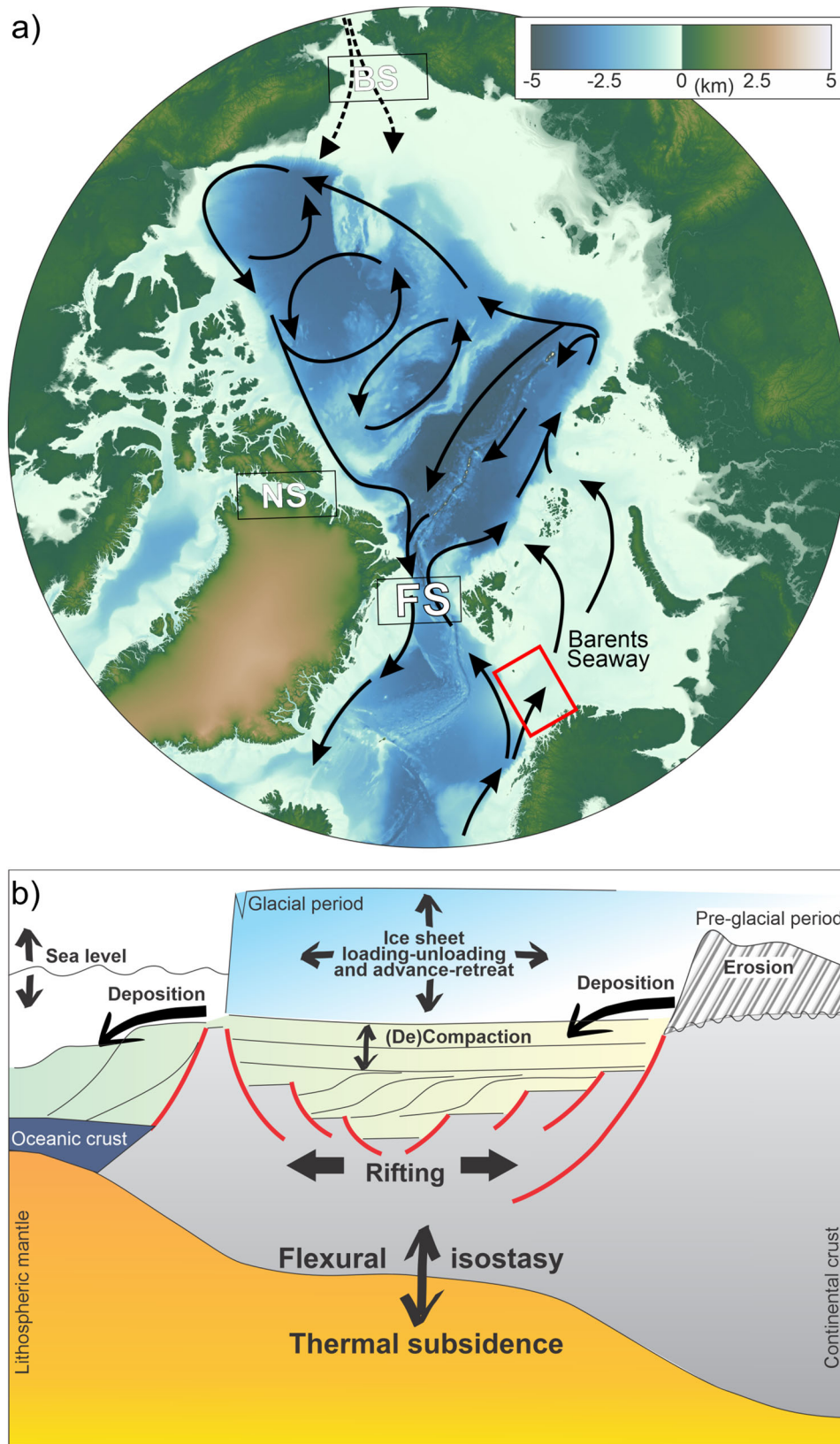


Fig. 1 The circum-Arctic and a conceptual cross-section of its continental margins. **a** Present-day bathymetry and topography of the Arctic derived from GEBCO⁵ database (modified from Jakobsson et al.⁴). Black arrows show the present-day, simplified ocean circulation. Dashed arrows show the Pacific Water influx through the Bering Strait (BS). Red rectangle represents the location of study area and Fig. 2. FS Fram Strait; NS: Nares Strait. **b** Schematic figure showing key factors that may influence the evolution of glaciated continental margins.

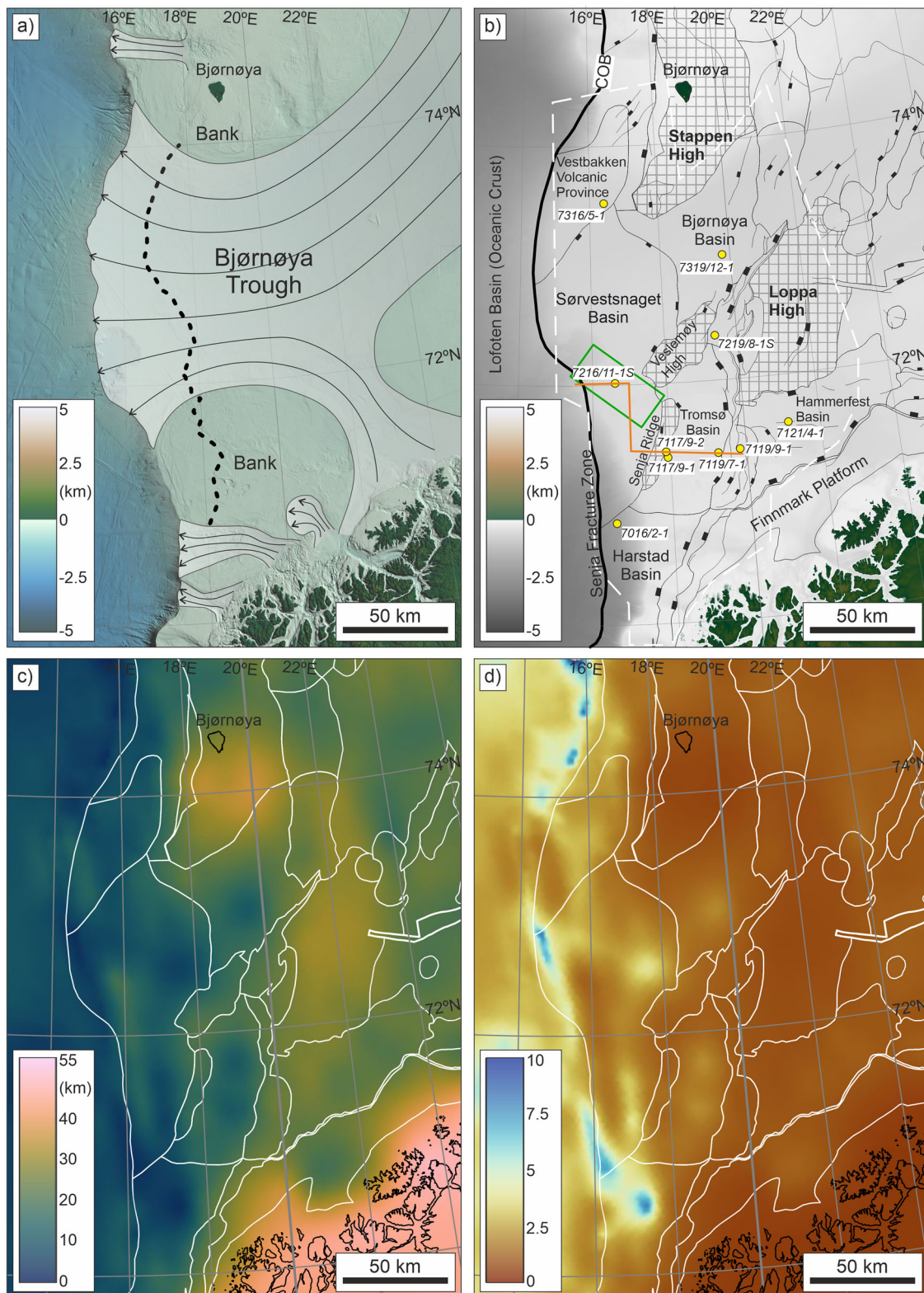


Fig. 2 The study area overlain by different characteristics and parameters. **a** Present-day seafloor morphology showing troughs (with ice stream flowlines) and banks in the SW Barents Sea. Dashed line represents the “hinge line” marking the boundary between net glacial erosion to the east and deposition to the west. **b** Major faults and structural elements in the SW Barents Sea (adapted from the Norwegian Petroleum Directorate), consisting of a series of highs and basins. Hatched areas represent the structural highs. Location of the representative seismic line in Fig. 3a (shown in orange) and well data (in yellow) is shown. The green rectangle represents the location of the 3D seismic data. White dashed line is the extent of seismic data used in this study (from Lasabuda et al.¹⁴). **c** Thickness of crystalline crust is adapted from Klitzke et al.⁵². **d** Beta factor map (dimensionless) assuming a crustal thickness of 25 km prior to the final rift phase leading to breakup at the Palaeocene-Eocene transition (see text for further details). COB: Continent-Ocean Boundary.

topography in SW Barents Sea at five periods: the Eocene (c. 55 Ma, 47 Ma), Oligocene (c. 33 Ma), Miocene (c. 20 Ma), and the onset of the Quaternary (c. 2.7 Ma), (ii) to estimate best-fit parameters associated with 3D flexural backstripping, reverse thermal subsidence and decompaction process, and (iii) to discuss the implications of the reconstructed paleobathymetry-topography on the evolution of large-scale Atlantic–Arctic water circulation.

Results and discussion

Our paleobathymetric and -topographic reconstructions cover an area where Paleocene to Quaternary strata are present. For the larger parts of the Barents Sea Paleocene–Miocene/early Pliocene are largely missing, therefore, our analysis of paleo-highs and lows for the wider Barents Sea is based on existing literature.

Early Eocene (55 Ma) reconstruction. The early Eocene paleobathymetry shows a predominantly shallow marine environment in the Tromsø Basin, Harstad Basin, Sørvestsnaget Basin, Vestbakken Volcanic Province, Hammerfest Basin, and a subaerial environment in the intrabasin highs (i.e., Senja Ridge and Veslemøy High) (Fig. 4a). The well 7117/9-2 in Senja Ridge shows a very thin or severely eroded lower Eocene interval, which supports our early Eocene reconstruction map (Fig. 4a). Lower Eocene marine strata (outer neritic—upper bathyal with range from 100–500 m) based on well 7316/5-1 in Vestbakken Volcanic Province^{56,57} and 7216/11-1S in Sørvestsnaget Basin²⁰ are in line with our reconstruction. Our palaeogeography which shows paleo-water depth (PWD) of 400 m at well 7316/5-1 and PWD of 450 m at well 7216/11-1S is also matched by recent basin modelling results⁵⁵ that show the Vestbakken Volcanic Province as submarine and large parts of the Tromsø Basin as shallow marine with PWD of 100–400 m. The SW part of the Loppa High and NW part of Finnmark Platform appear partly subaerial (Fig. 4a), which is in agreement with seismic analysis by Knutsen and Vorren⁵⁸.

For regional paleogeographical development in the Barents Seaway in the early Eocene (c. 55 Ma), a recent paleo-stress analysis⁵⁹ shows that far-field stress may propagate to the northeastern part of the study area, leading to a development of paleotopographic highs, including anticlines and domes (e.g. Storbanken High). Other regional studies and source-to-sink analyses also suggest a subaerial paleo-Barents Sea to the east^{14,60}.

Middle Eocene (47 Ma) reconstruction. The middle Eocene paleobathymetry shows major rift-related deepening compared to the early Eocene map. The northern Sørvestsnaget Basin shows a gradual depression that created basin accommodation for sediments to accumulate. Seismic data suggest a clinoform development sourced from the nearby Stappen High^{14,61}. This finding is supported by muddy and sandy turbidite fans described from core data at well 7216/11-1S suggesting a deepwater paleoenvironment^{57,61}. A deep marine shale interval at well 7316/5-1 in Vestbakken Volcanic Province also fits with our reconstruction that shows a PWD of 1000 m at this well location. Deep marine conditions (bathyal environment of up to 2000 m, Fig. 3b) also occurred in Sørvestsnaget and Tromsø Basins which are matched with our PWD of 800 m at well 7216/11-1S. Meanwhile, large parts of the Senja Ridge and Veslemøy High appear to be subsided and drowned (PWD of 50–300 m) but still sitting at a higher level compared to the surrounding basins, while other parts remain subaerial (paleotopographic of 30 m at well 7117/9-2 in Senja Ridge) (Fig. 4b). This observation agrees well with a tectonostratigraphic restoration using seismic data for this area²⁰.

For a wider Barents Sea in the middle Eocene (c. 47 Ma), a source-to-sink study for the Cenozoic strata¹⁴ shows that there may have been paleotopographic highs to the east and north of the study area, where sediment progradations have been observed from seismic data in the Tromsø Basin and Sørvestsnaget Basin. This palaeogeography is also in agreement with a regional Eocene map⁶⁰, which suggest a closed Barents Seaway for the entire Eocene.

Oligocene (33 Ma) reconstruction. The Oligocene paleobathymetry shows a major marine basin shallowing in the Sørvestsnaget Basin (two times shallower than in the middle Eocene) and Vestbakken Volcanic Province (PWD of 400 m at well 7316/5-1), which largely fits with well data^{20,57,62} (Fig. 4c). The Hammerfest Basin appears to be subaerial (up to 500 m a.s.l.). However, large parts of the Senja Ridge and Veslemøy High remain submerged (PWD of 100–300 m) like for the preceding middle Eocene period. This morphology may be explained by high erosion of these structural highs to the adjacent basins during the middle Eocene that resulted in thick middle-upper Eocene strata based on observation from seismic data (Fig. 3a). The overall basin shallowing and considerable erosion of exposed structural highs could be related to major sea-level fall in the Eocene–Oligocene transition¹⁹ and/or an uplift episode due to major changes in plate movement, which is also observed regionally in the Barents Sea¹². This uplift is likely associated with a mantle rise and lithospheric thinning, volcanism and rift-flank uplift, whose rates are likely higher in areas along the continental margin¹².

Our paleobathymetric map suggests an easterly extent of the Oligocene strata that covered Tromsø Basin, Veslemøy High, parts of Hammerfest Basin and Bjørnøya Basin (Fig. 4c). This is in line with the paleogeographical reconstruction using a mass balance analysis¹⁴ that suggested a paleoenvironment of shallow marine to shelf in Tromsø Basin, Sørvestsnaget Basin, and a fluvial to coastal plain paleoenvironment in Hammerfest Basin and Bjørnøya Basin to the east.

Miocene (23 Ma) reconstruction. The Miocene paleobathymetry shares an overall similar morphology with the Oligocene. The Tromsø Basin (PWD 200–500 m based on our reconstruction) and Vestbakken Volcanic Province (PWD of 500 m at well 7316/5-1) appear to be dominated by shallow marine environments (Fig. 4d), while the Sørvestsnaget Basin shows rather deeper marine (PWD of 900 m at well 7216/11-1S), which is contrary to the shallow marine well interpretation of Ryseth et al.²⁰. We suspect that this part of the Sørvestsnaget Basin was formed into slope morphology during this time where contourites are found²⁸. The structural highs (e.g., Senja Ridge, part of Veslemøy High, and part of the western flank of the Loppa High) and the Hammerfest Basin were predominantly positive features (up to 500 m a.s.l.).

Further to the east and north, this part of the Barents Shelf is suggested to have been subaerially exposed based on regional modelling and mass balance analysis^{8,14,63}. Although some studies have suggested an open Barents Seaway sometime in the Miocene^{1,64,65}, we find a mainly subaerial paleo-Barents Sea based on our sensitivity tests (see below), with all tested parameters indicating an eastward shallowing trend that led to a subaerial Barents Shelf. Our reconstruction is also in line with the available core data⁶⁶ and well data from the Vestbakken Volcanic Province⁶² that show shallow marine environments (0–500 m). The northwestern part of the Barents Shelf (i.e., Svalbard) is considered a highland throughout the Miocene^{1,8,64}, where an initial ice cap is suggested to have formed at c. 14 Ma⁸.

Table 1 Compilation of previous modelling results (and this study) regarding the paleogeographical evolution of the Barents Seaway, model resolutions, modelling scales and corresponding references.

Barents Seaway	Time slice	Paleobathymetry specifically at the SW Barents Sea	Did the Atlantic Water enter the Barents Seaway?	Model resolution	Modelling scale	Reference
Barents Seaway close	55 Ma	Partly subaerial	No	750 × 750 m	Local SW Barents Sea	This study
	47, 33, 20 and 2.7 Ma	Submarine to subaerial	No	750 × 750 m	Local SW Barents Sea	This study
	1.5 and 0.7 Ma	Partly subaerial	No	10 × 10 km	Local SW Barents Sea	Zieba et al. ¹⁶
	2.3 and 1 Ma	Subaerial to partly subaerial	No	50 × 50 km	Regional Barents Sea	Butt et al. ¹⁵
	14 Ma	Subaerial	No	low resolution	Regional Barents Sea	Knies and Gaina ⁸
	3 Ma	Subaerial	No	low resolution	Regional Barents Sea	Dimakis et al. ²⁴
	2.6 Ma	Partly subaerial	No	10 × 10 km	Regional Barents Sea	Amantov and Fjeldskaar ⁶⁷
	from 66 to 11 Ma	Subaerial	No	5 arc min (c. 9 × 9 km) 6 arc min (c. 11 × 11 km)	Global	Straume et al. ¹
	60 and 20 Ma	Subaerial	No	10 × 10 km	Global	Poblete et al. ⁷³
Barents Seaway open	0.7 and 0 Ma	Submarine	Yes	low resolution	Local SW Barents Sea	Zieba et al. ¹⁶
	2.7 and 0 Ma	Submarine	Yes	50 × 50 km	Regional Barents Sea	Rasmussen and Fjeldskaar ⁶⁸
	1 Ma	Submarine	Yes	low resolution	Regional Barents Sea	Butt et al. ¹⁵
	15 Ma	Submarine	Yes	low resolution	Global	Herold et al. ⁶⁴
	from 11 to 0 Ma	Submarine	Yes	9 × 9 km	Global	Straume et al. ¹
	40 Ma	Submarine	Yes	6 arc min (c. 11 × 11 km)	Global	Poblete et al. ⁷³

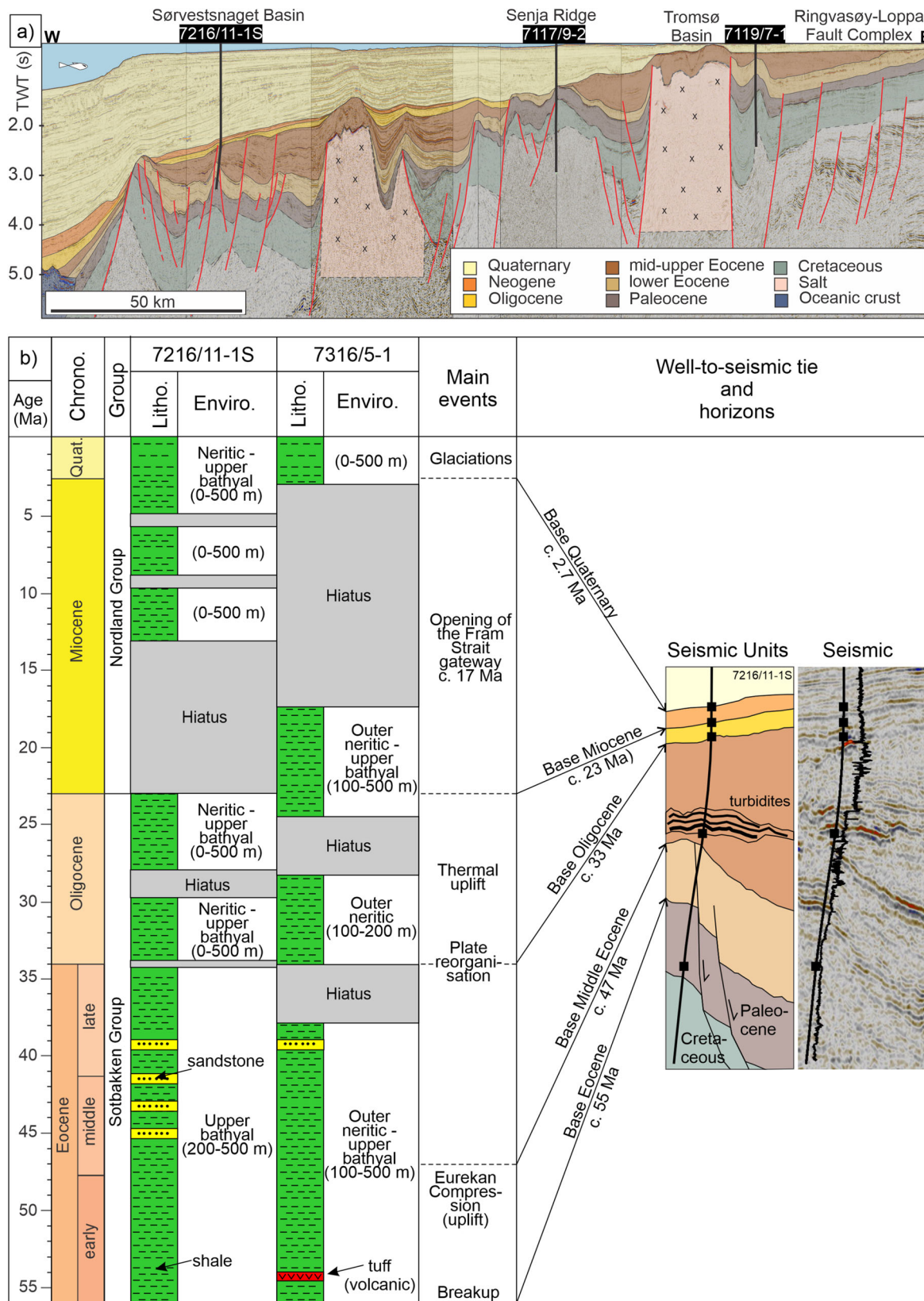


Fig. 3 Stratigraphy from seismic and well data. a Seismic profile showing the sediment fill and structural style in SW Barents Sea (modified from Lasubada et al.¹⁴). **b** Eocene to recent lithology and paleoenvironmental interpretation from wells 7216/11-1S and 7316/5-1 based on an updated biostratigraphy analysis by Eidvin et al.⁵⁷. Seismic horizons and age estimates tied to well 7216/11-1S are shown. For location of seismic profile, see Fig. 2b.

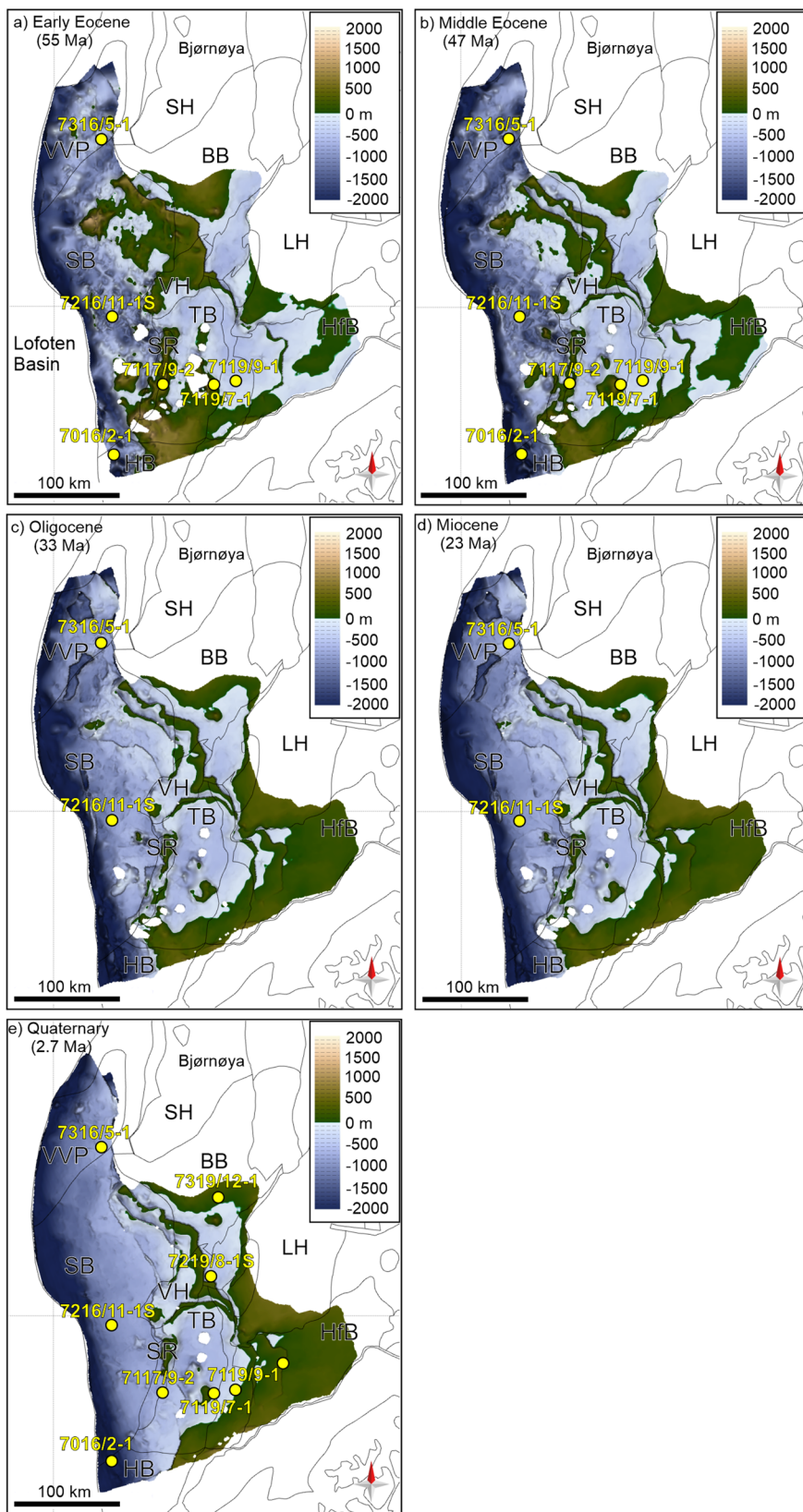


Fig. 4 Paleobathymetric-topographic reconstructions of the SW Barents Sea. **a** Early Eocene c. 55 Ma, **b** Middle Eocene c. 47 Ma, **c** Oligocene c. 33 Ma, **d** Miocene c. 23 Ma, and **e** Quaternary c. 2.7 Ma. The yellow circles in each figure represent the well control points where the corresponding interval is present. These figures were generated using an academic license of MOVE, therefore they were not produced for commercial use. VVP: Vestbakken Volcanic Province; SH: Stappen High; BB: Bjørnøya Basin; SB: Sørvestsnaget Basin; VH: Veslemøy High; SR: Senja Ridge; TB: Tromsø Basin; LH: Loppa High; HfB: Hammerfest Basin.

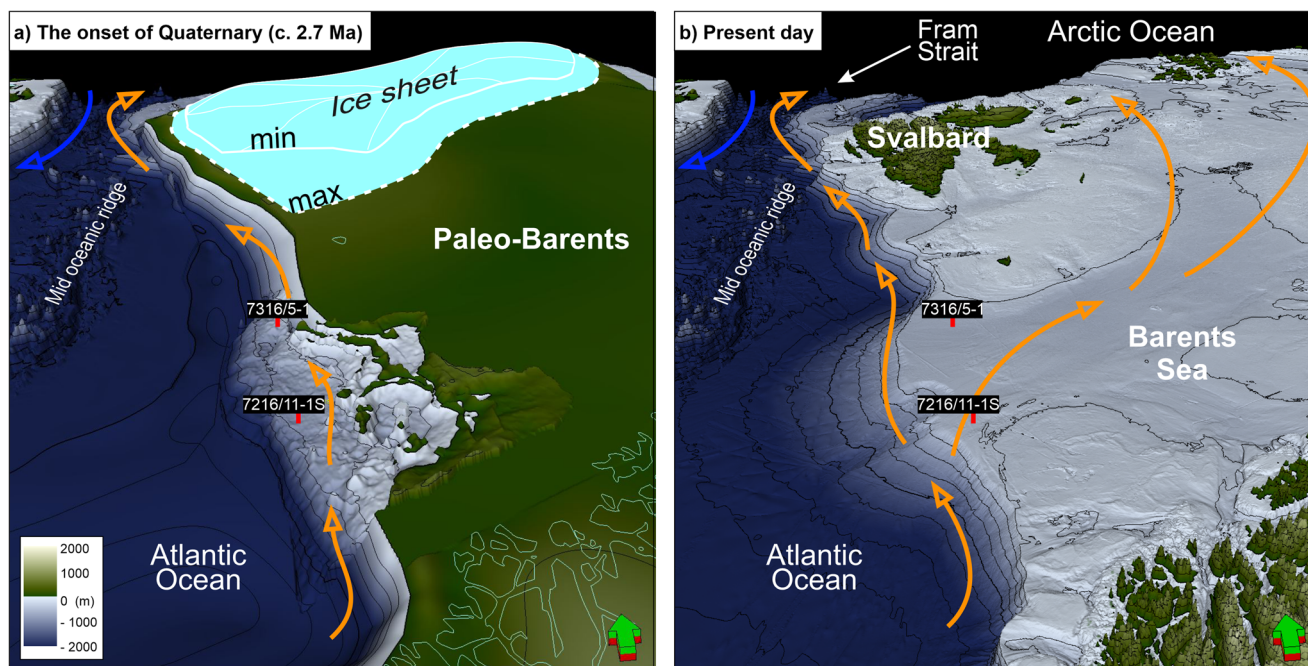


Fig. 5 Barents Seaway in two different times. **a** 3D conceptual model of Atlantic–Arctic water circulation at the onset of Quaternary (c. 2.7 Ma). The reconstruction for the wider Barents Sea to the east follows Butt et al.¹⁵. Minimum–maximum ice sheet extent is based on Knies et al.³⁵. **b** Present-day bathymetry of Barents Sea. Orange arrows represent water current of Atlantic origin. Blue arrows represent water current of Arctic origin.

Quaternary (c. 2.7 Ma) reconstruction. The paleobathymetric–topographic reconstruction at the onset of Quaternary is relatively similar to the early Miocene, displaying a predominantly shallow marine environment (PWD of 600 m at well 7316/5-1), slope morphology (PWD 900 m at well 7216/11-1S) and a subaerial topography to the east in the SW Barents Sea area (Fig. 4e). However, a smoother seafloor morphology is observed in most of the basinal parts. The shelf–slope transition is still present towards the west. The subaerial parts are mostly located in Hammerfest Basin (200–300 m a.s.l) and parts of Loppa High (up to 500 m a.s.l), as well as in basin margin areas.

Seismic mapping studies^{28,45} indicate a continued influx of Atlantic Water in the western margin of Barents Sea during this time. In areas farther east and north, the Barents Shelf is interpreted as a subaerial lowland based on a source-to-sink study³⁹, regional modelling^{15,24,32,67}, studies of upper slope processes³⁴, and seismic mapping⁵⁸ (Fig. 5a). However, a shallow water connection is suggested to exist at the Barents Seaway based on older data and modelling⁶⁸. The shallow marine environments that existed between highs (i.e., paleo-Hammerfest Basin and paleo-Stappen High) may represent a favourable area for focused glacial erosion, which led to the development of Bjørnøya Trough where ice streams intensively eroded the substrate during Quaternary glaciations^{34,37}.

Implications for Atlantic–Arctic ocean circulation. There is a general consensus on the early Miocene opening (c. 17 Ma) of the Fram Strait^{4,10} although an earlier (Eocene) inflow of Atlantic Water to the Arctic Ocean is also feasible⁶⁹. The estimated timing of the opening of the Barents Seaway however, varies by millions of years. These discrepancies are mainly related to the resolution of the model applied (i.e., 100’s m vs 10’s km grid spacing), focus of the study (i.e., local versus regional Barents Sea or global), and the methods applied (e.g., Airy model vs flexural model). For example, although implementing an updated workflow and database, the focus of modelling by Straume et al.¹ is on the opening of deep, oceanic

gateways (e.g., Fram Strait) instead of shallow, continental seaways (e.g., the Barents Seaway). A review of previous work on the Barents Seaway and its southern inlet (the SW Barents Sea) is summarized in Table 1. Below, we discuss the implication for the timing of opening of the Barents Seaway from our high-resolution model and other more regional studies, and its implications to the Atlantic–Arctic water circulation.

The Eocene. At the Paleocene–Eocene transition (c. 55 Ma), our paleotopographic reconstruction appears to hinder water inflow through the Barents Seaway from the Atlantic. There may have been a connection between the Arctic and Atlantic Ocean as indicated by the Azolla event (~49–48 Ma) recorded in the ACEX drilling and other wells on the NE Atlantic margin⁷⁰. However, these Azolla records appear to be linked to climatic conditions (at a thermal maximum) rather than an overflow of freshwater from the Arctic Ocean. This overflow, if it occurred, however, could not have been through the Fram Strait, which was not open or even formed yet due to a major compression in the area that formed the Eureka–West Spitsbergen fold–thrust belt^{26,71}. Therefore, a connection across the eastern Barents Shelf and/or Turgay Strait⁷² is here considered most likely.

Subsequent subsidence of the basins and drowning of structural highs in the middle Eocene (c. 47 Ma) in the SW Barents Sea may indicate a shallow water passage that allowed Atlantic Water to enter the Barents Seaway. However, there may have been paleotopographic highs existing to the east and north of the study area that blocked the connection between water masses^{14,59,60} (see discussion above). How deep and wide this connection eventually was, and to what extent it was involved in North Atlantic–Arctic water exchange, is not clear from the present study. An open Barents Seaway was previously postulated for the entire Eocene using sparse data from mainly Scandinavia⁶³, and at c. 40 Ma based on global paleogeographical modelling⁷³. However, from a regional mass balance analysis¹⁴ and global paleogeographical modelling¹, the Barents Seaway is suggested to be closed for the entire Eocene.

Recent ocean circulation and climate modelling⁷⁴ also indicate a closing of Barents Seaway and shallow opening of the Fram Strait at the end of Eocene, which contributed to global cooling (see below). Thus, we support a closed Barents Seaway during the entire Eocene⁶⁰, although, based on our results alone, we cannot exclude the interpretation of an open, “proto” Barents Seaway during the middle Eocene (possibly linked to the Turgay Strait), followed by a gradual closing of this seaway during the late Eocene and full closure in the Oligocene. More detailed timesteps are clearly needed to reveal the exact development scenarios of the Barents Seaway during this time interval.

The Oligocene. Our reconstruction for the earliest Oligocene (c. 33 Ma) shows paleotopography that may have formed a barrier for Atlantic Water passing through the Barents Seaway. A closed Barents Seaway is also supported by a recent study based on a regional mass balance analysis¹⁴ and a global paleogeographical modelling¹. The implication of a closed Barents Seaway and Fram Strait⁴, or at least a very shallow and narrow Fram Strait^{1,10} and thus, an isolated Arctic Ocean has been discussed by Hutchinson et al.^{3,75}, who linked these configurations to major warming of the North Atlantic Ocean and cooling of the North Pacific at the Eocene–Oligocene Transition (EOT). These temperature changes can be explained by Atlantic meridional overturning circulation due to a lack of freshwater inflow from the Arctic, i.e., a closed Barents Seaway³. At the global scale, these events may have lowered global CO₂ levels that led to the development of an Antarctic ice sheet in the Oligocene⁷⁵.

The Miocene. Our paleobathymetric map (c. 23 Ma) shows an overall eastward shallowing trend, incorporating a deep-marine area to the west and a subaerial landscape to the east. Consequently, sediments are inferred to have been transported from eastern and northern source areas toward shallow marine and to deeper marine to the west and southwest in the Barents Sea area. Our Miocene reconstruction is in line with the regional sediment transport pattern and processes based on seismic mapping^{14,76}. Furthermore, well data from 7216/11-1S and 7316/5-1 (on the paleo-slope) show predominantly muddy contouritic strata for the Miocene interval, while 7316/06-U-01 further east (paleo-shelf) includes a sandstone interval of early Miocene age^{57,66}. The dominance of muddy contourites on the slope implies little run-off from the SW Barents Sea area (i.e., distant sediment source area) with eastern and northern positive topographies of Miocene age blocking the inflow of Atlantic Water.

In the Vestbakken Volcanic Province and Sørvestsnaget Basin, seismic stratigraphic analyses show contouritic strata suggesting that Atlantic Water passed the study area northwards since the Miocene²⁸. The external character (geometry) of contourites on the slope suggests a development of moat and drift²⁸ that are associated with stronger currents and often found on a slope⁷⁷. If the Barents Seaway was open and water could flow through the Fram Strait like today, the slope would have been dominated by a different type of contourites than of Rydningen et al.²⁸, for example sand-rich (sheet-like) contourites that would indicate a closer distance to the sediment source area⁷⁸.

The Quaternary. Our modelling results in the SW Barents Sea, combined with previous regional modelling to the east (see Table 1), suggest that the Barents Seaway did not exist at the onset of the Quaternary (c. 2.7 Ma) (Fig. 4e). This finding means that the modern Barents Seaway opened sometime after c. 2.7 Ma. This configuration also implies that at the onset of the Quaternary, Atlantic Water must still have bypassed the SW Barents Sea area and flowed northwards towards the Fram Strait, the only gateway at this time (Fig. 5a). The predominantly subaerial

environment in the greater Barents Sea regions is in some studies suggested to have persisted until 1.5 Ma, and that the Barents Seaway opened later at c. 1–0.7 Ma^{15,16,24}.

A recent ice sheet reconstruction by Hjelstuen and Sejrup³⁸ shows major expansion after 1.5 Ma until at least 0.5 Ma, where ice-sheets covered extensively from Svalbard to the southern coast of Norway including the Barents Sea. These massive ice-sheets would have temporarily hindered connection between both water masses from the Atlantic and from the Arctic via the Barents Seaway. This shelf-wide ‘blocking’ by ice-sheets, including in the SW Barents Sea, persisted through to the Last Glacial Maximum c. 20 ka based on a regional glacial sediment correlation⁴¹. Note that ice sheets have expanded and reduced/disappeared as well as advanced and retreated multiple times during each glacial cycle, affecting the regional ocean circulation throughout the Quaternary.

The presence of the Quaternary ice sheets across Eurasia led to a shelf-wide increase in the rate of erosion^{32,38}. This erosion, primarily beneath fast-flowing ice streams, deepened the SW Barents Sea area, as reflected by the present-day trough morphology, the thickness of the glacial sediment depocentres adjacent to the major through mouths^{34,38}, and the overall depth of the Barents Sea today (c. 200 m in average). Continental slope contourites²⁸ documented an interaction of drift with glacial debris that show an interplay between a northward flow of Atlantic Water and glacially induced gravity-driven processes during the Quaternary. As a result of the opening of the Barents Seaway sometime after 2.7 Ma, gradually more water is interpreted to have passed through the Barents Seaway during the Quaternary interglacials (Fig. 5b) while the inflow of Atlantic Water through the Fram Strait reduced, assuming a constant volume of Atlantic Water entering the NE Atlantic from the south. An oceanographic modelling approach is needed to further clarify the implications of this evolving configuration.

Conclusions

This study addresses the history of Atlantic Water inflow to the Arctic Ocean through the Barents Seaway from the Eocene through to the Quaternary at five time periods (c. 55 Ma, 47 Ma, 33 Ma, 20 Ma, and 2.7 Ma). The key results can be summarized as follows:

- We present high-resolution paleobathymetric/-topographic reconstructions using better constrained input from surfaces based on seismic data, calibration from well databases, and key parameters (e.g., thermal subsidence, flexural isostasy and decompaction) in a sequential “back-stripping” process.
- At the earliest Eocene (c. 55 Ma), the subaerial topography of paleo-SW Barents Sea was likely enough to block Atlantic Water from entering the Barents Seaway. Major basin subsidence and deepening of the structural highs at c. 47 Ma may later have allowed Atlantic Water to enter this part of the Barents Seaway (i.e., SW Barents Sea) but then likely became blocked by paleo-highs to the east of the study area.
- At c. 33 Ma, 20 Ma, and 2.7 Ma, basin shallowing and regional shelf uplift indicate a continued blockade to Atlantic Water entering the Barents Seaway, with a gradual deepening from predominantly shallow marine to deeper marine environments towards the west.
- Our paleobathymetric-topographic reconstructions help to constrain the opening of the Barents Seaway to after c. 2.7 Ma. However, a more detailed chronologically based modelling is needed to better constrain the exact opening of the Barents Seaway during the Quaternary.

- After the onset of the Quaternary (c. 2.7 Ma), the present Barents Sea was affected by profound glacial erosion and deepening. As a result, the area has gradually transformed from a subaerial to a submarine platform that allowed for a progressively increasing inflow of Atlantic Water across the Barents Seaway and into the eastern Arctic Ocean. Consequently, inflow of Atlantic Water through the Fram Strait reduced, assuming a constant volume of Atlantic Water entering into the Arctic.

Methods and uncertainties

Seismic horizon preconditioning. We used seismic horizons from Lasabuda et al.¹⁴ for the Base Paleocene (c. 66 Ma), Base Eocene (c. 55 Ma), Base Mid Eocene (c. 47 Ma), Base Oligocene (c. 33 Ma), Base Miocene (c. 23 Ma) and Base Quaternary (c. 2.7 Ma) paleosurfaces (Fig. 6). The TWT (two-way travel time) surfaces were converted to depth (m) using the TGS J-Cube velocity model. An uncertainty for this velocity model might be related to locally sparse seismic data in the westernmost part of the study area. However, the velocity cube has been calibrated with a number of iterations using regional seismic and well data to ensure its high-quality standard. The salt diapirs²⁰ were not taken into consideration due to their local distribution to simplify modelling iteration without losing the integrity of the modelling steps (i.e., as shown in Fig. 7).

Backstripping workflow. The backstripping technique using the 3D MOVE numerical software incorporates decompaction using a porosity–depth curve⁷⁹, thermal subsidence history⁸⁰ and flexural isostasy^{50,51}. The workflow performed in this study started with the present-day stratigraphic configuration consisting of the Cenozoic pre-glacial sediments overlain by glacial sediments (Fig. 7a). We removed the glacial sediments, then applied the decompaction step and restored the flexural isostasy (Fig. 7b). We reconstructed the missing part of the lower-middle Cenozoic strata by interpolating their surfaces onto the shelf using the thickness attribute module in MOVE (Fig. 7c).

When interpolating the base of Quaternary from the slope to the shelf, we defined a “hinge line” at the onset of glacial TMF growth (see Fig. 7a). This line represents a boundary between net glacial erosion to the east and glacial deposition to the west of this line (Fig. 2a).

Our surface interpolations towards the shelf correspond to a total missing thickness of c. 1175 m, which consists of Miocene (138 m), Oligocene (168 m), mid-Eocene (426 m), lower Eocene (200 m), and Paleocene (242 m) (Fig. 7c). This total thickness of missing sediments was distributed evenly on the shelf part of the study area, representing the glacial trough, where the study area is mostly located. This number fits well with the mass balance calculation for the glacial erosion in the Bjørnøyrenna Trough, which has been estimated to be c. 1000–1100 m³⁷.

After adding subsidence due to the weight of the restored sediments on the shelf, the paleobathymetry for the onset of Quaternary (c. 2.7 Ma) was reconstructed (Fig. 7d). Based on similar steps (i.e., removal of a layer, decompaction and flexural isostatic compensation), the paleobathymetry at the onset of Miocene (c. 23 Ma) was also reconstructed (Fig. 7e, f) before the middle Eocene (c. 47 Ma) and early Eocene (55 Ma) paleobathymetry were reconstructed.

Numerical model setup and sensitivity test. Due to computational limitations, there are some assumptions in this modelling. (1) We run the model on the continental crust, i.e., the oceanic crust is not included (Fig. 1b). Although the study area is located on the plate margin, where it is thinner, we assume that we are

Table 2 Parameters for modelling the reverse thermal subsidence and flexural isostatic response.

Modelling step	Parameter	Value	Unit
Reverse thermal subsidence modelling	Rifting age	66	Ma
	Syn-rift duration	10	Ma
	Sediment density in thermal subs modelling	2200	kg/m ³
Flexural isostatic restoration modelling	Lithospheric thickness*	60	km
	Crustal thickness*	25	km
	Effective elastic thickness (T_e)	5	km
	Young modulus	103000	MPa
	Poisson's ratio	0.25	unitless
	Nyquist wavelength	10000	m
	Sediment density	2200	kg/m ³
	Water density	1025	kg/m ³
	Mantle density	3300	kg/m ³

*prior to final rift phase leading to breakup.

working with much of the full thickness of the lithosphere. We mitigate this uncertainty by testing three different lithosphere thicknesses (see below). (2) We also assume a homogenous lithosphere and crust, although, these are likely to be spatio-temporally heterogenous in thickness and rheology⁸¹.

We run our model using a c. 750 × 750 m grid spacing, which, as far as we are aware, is the highest model resolution applied in this region (Table 1). In this section, we highlight three key factors that are considered in this numerical modelling: thermal subsidence, flexural isostasy, and decompaction (Fig. 1b).

Thermal subsidence. Thinning of the lithosphere due to rifting allows for the hot asthenosphere to rise in the mantle. When rifting ends, the mantle material cools and becomes part of the mechanically rigid lithosphere, becoming denser and eventually sinking, enhancing the subsidence magnitude of the sedimentary basin. The effect of thermal subsidence exponentially decreases through time and lasts for about 100 Myrs⁸⁰. Therefore, the effect of thermal subsidence due to rifting during the Paleocene–Eocene in the SW Barents Sea area will interfere with the effect of isostatic uplift, which has been accounted for during the modelling. We set the onset of rifting to 66 Ma (at the beginning of Paleocene), with a time span of 10 Myrs, i.e., until the approximate initiation of the breakup⁸² (Table 2). The uncertainty here may be related to a prolongation of the rifting period locally, e.g., Vestbakken Volcanic Province and part of the Sørvestsnaget Basin, where extension may have extended into Oligocene time¹³.

Flexural isostasy. The flexural isostasy model promotes the importance of regional compensation of the load considering the rigidity and strength of the lithosphere⁸¹. Flexural isostasy considers the crust as a visco-elastic plate, which responds to any perturbation on the load due to tectonics (e.g., compression–extension, uplift–subsidence) and surface processes (e.g., erosion–sedimentation, sediment loading–unloading). Ice sheet loading–unloading is relatively short-lived across geological timescales (c. tens of thousands of years) and therefore we only consider the tectonic effects that resulted from erosion and redistribution of sediments (Fig. 4). However, considering repeated loading pulse and dynamics of ice sheet advance and retreat, there could be an effect of overcompaction stages, leading to a slightly underestimated decompaction value which may be difficult to account for⁸³.

We applied a flexural isostatic correction instead of the Airy model due to the size of the study area being large enough

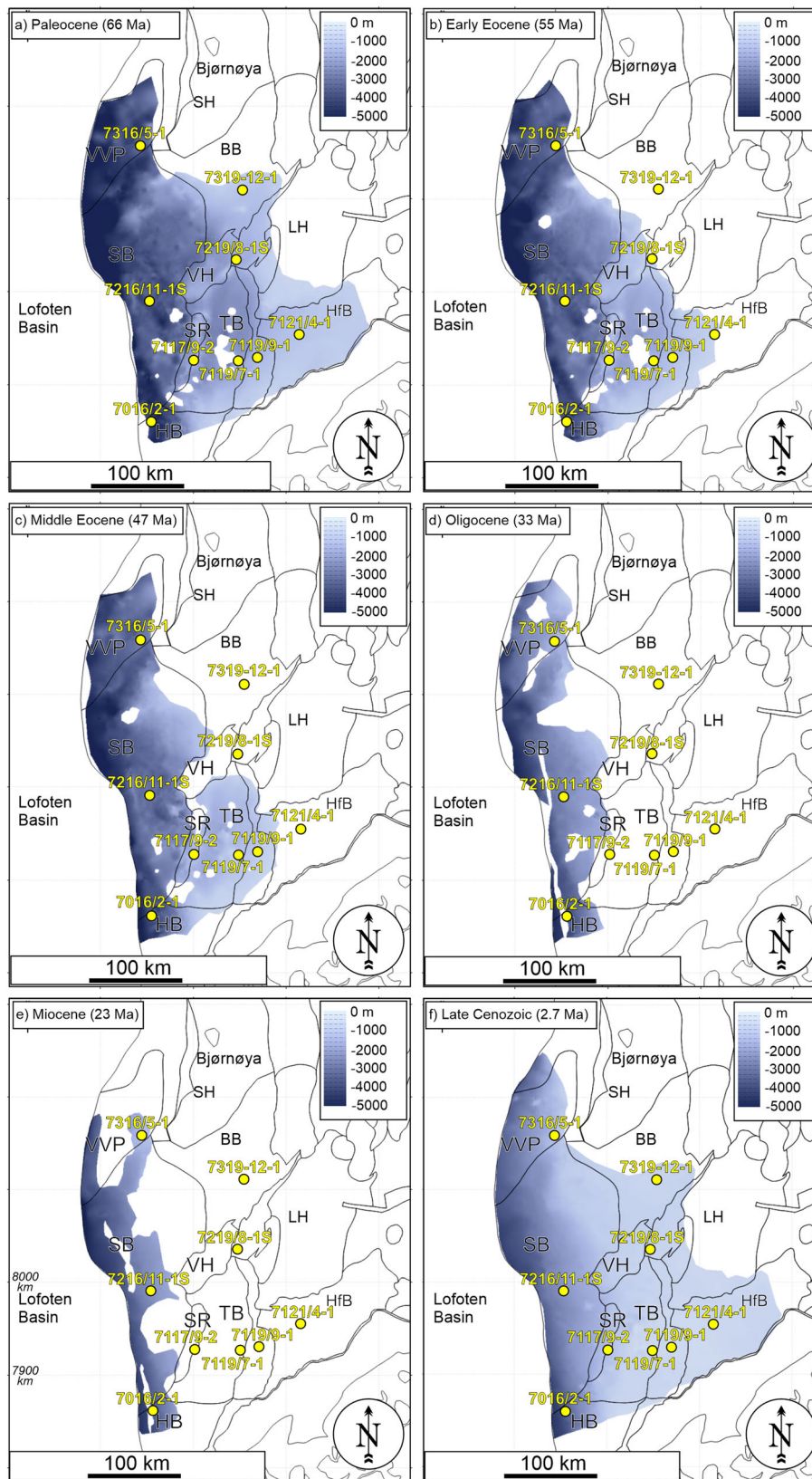


Fig. 6 Depth-converted surfaces that were used in the modelling workflow. **a** Base Paleocene c. 66 Ma, **b** Base Eocene c. 55 Ma, **c** Base Middle Eocene c. 47 Ma, **d** Base Oligocene c. 33 Ma, **e** Base Miocene c. 23 Ma, and **f** Base Quaternary c. 2.7 Ma. The yellow circles represent the well data. These figures were generated using an academic license of MOVE, therefore they were not produced for commercial use. VVP: Vestbakken Volcanic Province; SH: Stappen High; BB: Bjørnøya Basin; SB: Sørvestsnaget Basin; VH: Veslemøy High; SR: Senja Ridge; TB: Tromsø Basin; LH: Loppa High; HfB: Hammerfest Basin.

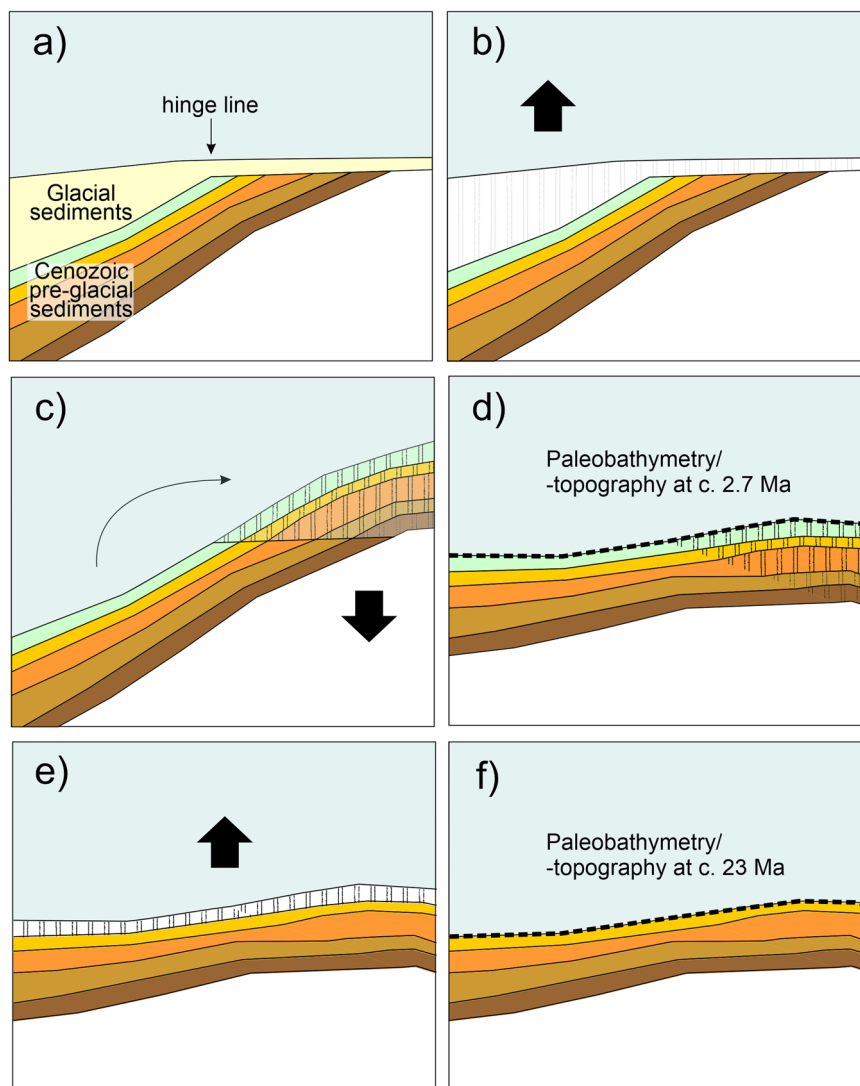


Fig. 7 Schematic steps of the sequential restoration (backstripping) workflow. **a** Present-day structural style and stratigraphic configuration in the study area. **b** Remove the glacial sediments, apply decompaction and restore the flexural isostasy. **c** Reconstruct the missing part of older Cenozoic strata by interpolating the surfaces onto the shelf. Restore the subsidence due to loading of reconstructed sediments on the shelf. **d** Paleobathymetry for the pre-glacial sediments at 2.7 Ma is reconstructed. **e** Apply the same approach (i.e., removal of each layer, decompaction and flexural isostatic compensation) to reconstruct the Miocene paleobathymetry. **f** Paleobathymetry at 23 Ma is reconstructed. Repeat steps **e**, **f** until the early Eocene paleobathymetry has been reconstructed. Terminology: below sea-level = paleobathymetry; above sea-level = paleotopography.

(c. 300 km width and length) to capture the flexure of the crust (Table 2). The flexural isostatic correction consists of weighing the initial lithospheric thickness h_0 with the ratio between densities of the crust, ρ_c , and the mantle, ρ_m to obtain⁸¹

$$h = h_0 \frac{\rho_c}{\rho_m} \tag{1}$$

The effective flexural rigidity (D) is defined as⁸¹

$$D = \frac{ET_e^3}{12(1-\nu^2)} \tag{2}$$

In Eq. (2), E is Young’s modulus of elasticity, T_e is the effective elastic thickness and ν is Poisson’s ratio. Flexural isostasy depends strongly on the effective elastic thickness (T_e) used in the model. The effective elastic thickness is an estimated thickness of an elastic layer which reflects the apparent strength of a loaded lithospheric plate.

We calculated the response for $T_e = 5, 10, 15, 20$ and 30 km. All T_e values show development of a deep marine

paleobathymetry during the Miocene in the Sørvestsnaget Basin that is consistent with well data (Fig. 8a). This result means that the T_e values are robust in this basin. However, in the Tromsø Basin the choice $T_e = 5$ km shows lower erosion, which is in better agreement with the erosion analysis by Lasabuda et al.¹⁴, and is thus considered as the best-fit parameter. The same parameter choice, $T_e = 5$ km has previously also been applied in the Barents Sea area^{54,55}, resulting in consistent modelling outcomes.

As the study area is located near the plate margin (i.e., close to a transform fault), we ran a sensitivity test to assess the best-fit value among three lithospheric thicknesses ($h_0 = 60, 70$ and 80 km). In previous large-scale modelling work of the greater Barents Sea, an initial lithospheric thickness of $h_0 = 120$ km is commonly applied to refer to the situation prior to the long-term multiphase rifting history (i.e., not just the final rifting phase leading to breakup in Paleogene)^{84,85}. Therefore, we did not include $h_0 = 120$ km in the sensitivity test. Our sensitivity tests using lithospheric thicknesses of $h_0 = 70$ and $h_0 = 80$ km support

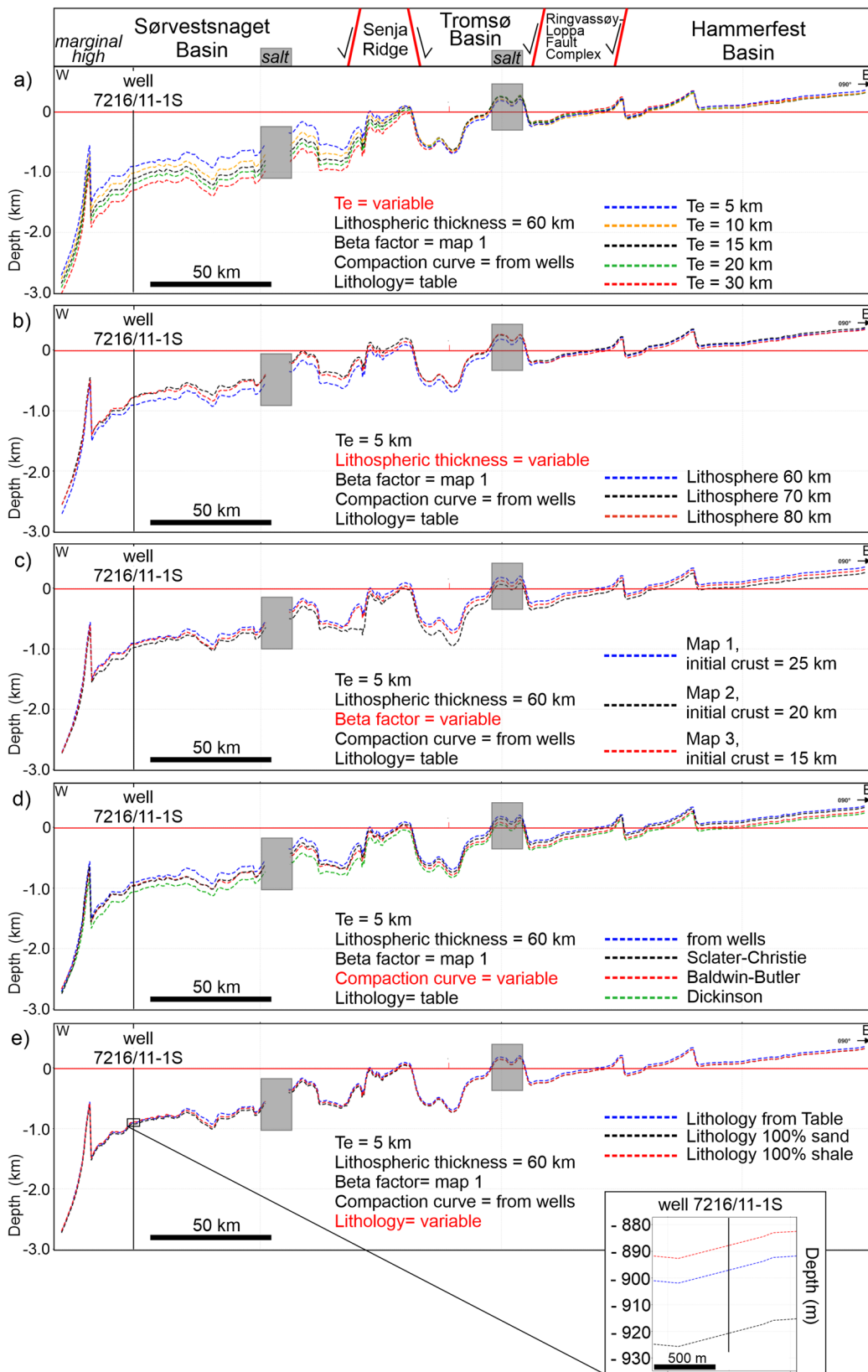


Fig. 8 Sensitivity test to investigate the effect of different parameters. **a** Effective elastic thickness (T_e), **b** lithospheric thickness, **c** Beta factor, **d** compaction curve, and **e** lithology with different initial thickness of the crust, on the restored Miocene paleobathymetry. For location, see orange line in Fig. 2b. These figures were generated using an academic license of MOVE, therefore they were not produced for commercial use.

this reasoning (multiphase rifting history) and gave unrealistic reconstructions (i.e., too much uplift), particularly for older strata (e.g., Eocene), which are inconsistent with available well data¹². Therefore, we choose the value of $h_0 = 60$ km which shows reasonable depth along the E–W transect of Miocene paleobathymetry (Fig. 8b). This value reflects a stretched continental margin following multiple rift phases over a long time span^{52,53} and this modelling addresses the final rifting episode in the Barents Sea, which may be valid reasons for this outcome.

For calculation of beta factors, we used a crustal thickness map from Klitzke et al.⁵² as this contains input from seismic data, which is a reliable constraint. We tested three initial thickness of continental crust ($h_0 = 25, 20$ and 15 km) before it was stretched in the final rift phase leading to breakup. They reflect the thickness of the crust at the onset of the final rift phase, which was already thinner (due to stretching/thinning associated with the earlier rift phases). Therefore, we did not include $h_0 = 35$ km as this value is a common reference thickness for the initial lithospheric extension assumed to happen in the late Palaeozoic. Our sensitivity test shows comparable depth variations of the three resulting Miocene paleobathymetries, particularly in the basin area (Fig. 8c). However, we chose a beta factor map that used an initial crustal thickness of $h_0 = 25$ km because it shows the most subaerial profile in the Hammerfest Basin to the east, which fits with a source-to-sink analysis¹⁴. This value represents a crust that has undergone a long-term multiphase rift evolution in the study area^{53,55,86}.

Decompaction. The decompaction procedure is a step to restore the porosity loss due to mechanical compaction during burial. A compaction curve represents a basin burial history, including net exhumation magnitude. The average porosity curve from well data located in basins which have experienced uplift on the Barents Shelf is compared to a ‘normal’ compaction curve from basins that experienced no or very little uplift, i.e., the North Sea⁷⁹ or using other curves^{87,88}.

The first step taken after removing the uppermost stratigraphic layer during the backstripping procedure is to decompact the underlying layers. The compaction here means a porosity reduction by both mechanical and chemical compaction (i.e., Quartz cementation). Decompaction parameters used are based on two average porosity–depth curves. The porosity ϕ was estimated from the bulk density ρ_b recorded by standard RHOB borehole logs according to

$$\phi = \frac{\rho_b - \rho_{ma}}{\rho_f - \rho_{ma}} \quad (3)$$

where ρ_{ma} is the density of the matrix, and ρ_f is the fluid density^{89,90}. We assumed that $\rho_{ma} = 2650$ kg/m³ and $\rho_f = 1000$ kg/m³.

The average lower erosion curve was based on well 7216/11-1S in the Sørvestsnaget Basin, 7117/9-2 in the Tromsø Basin, 7117/9-1 on the Senja Ridge and 7316/5-1 in the Vestbakken Volcanic Province, which are in close fit with the porosity–depth curve of Sclater and Christie⁷⁹ (Supplementary Fig. 1). The average higher erosion curve was based on wells 7119/9-1 in the Ringvassøy-Loppa Fault Complex (RLFC), 7016/2-1 in the Harstad Basin, 7121/4-1 in the Hammerfest Basin and wells 7319/12-1 and 7219/8-1S in the Bjørnøya Basin, but we did not use this curve as they show a thinner interval of Cenozoic strata that is not sufficient to create a reliable compaction curve.

We ran a sensitivity analysis by using different compaction curves (i.e., the one from well data, Sclater-Christie, Baldwin-Butler, and Dickinson curves, Fig. 8d). The Miocene paleobathymetric-topographic reconstruction using a compaction curve based on well data shows comparable depths with

reconstructions using Sclater-Christie and Baldwin-Butler curves, particularly in the westernmost basins (Fig. 8d).

Furthermore, we applied surface porosity, depth coefficient, shale volume, grain size and density parameters for the decompaction step based on inspection of well data (Supplementary Table 1) as well as parameters from previous work in this area^{16,52,54,55}. We specifically tested our lithological input based on Supplementary Table 1 against 100% sand and 100% shale to capture the effect of lithology in the resulting paleobathymetry-topography (Fig. 8e). The results show that 100% sand gives 30 m deeper depth while 100% shale gives 10 m shallower depths compared to the model using lithological inputs derived from wells (Fig. 8e).

Sea-level. Another uncertainty that is not directly addressed in the MOVE numerical software is the eustatic sea level. The long-term eustatic sea-level curve trend for the Miocene (c. 23 Ma) to Quaternary (c. 2.7 Ma) shows falling sea-level from c. 100 m to -100 m¹⁸. This means that the depth of the paleobathymetry for the Miocene is a minimum estimate as the sea level position may need to be adjusted up by to 100 m. Meanwhile, the depth of the Quaternary is a maximum estimate as depths may need to be reduced by up to 100 m. However, the eustatic sea-level variation estimated by Miller et al.¹⁹ is less pronounced, fluctuating with ranges from c. -50 to 50 m. Even if the sea-level was 100 m higher, the paleotopography to the east (outside our study area) will still be enough to block the Atlantic Water passing through the Barents Seaway. For the Oligocene–Miocene, the major shelf uplift to the east will still hinder the Atlantic–Arctic water connection. In summary, we did not alter the results of the paleobathymetry in this modelling, but we are aware of there may be a depth correction related to eustatic sea-level variations for future more-detailed denser-timespan reconstructions.

Dynamic topography. Another aspect that we have not assessed in detail is the dynamic topography, especially because our study area is located on the edge of the NE Atlantic. The residual topography estimation due to the arrival of the Iceland plume shows a diminishing pattern from 1350 to 1800 km away from Iceland⁹¹. However, this pattern may be different in older time episode, for example in the Eocene where Nordic Seas were narrower, and the plume were closer to the study area. This evolving pattern with respect to plate tectonics indicates that dynamic topography is an uncertainty in reconstructing paleobathymetry and -topography in our study area.

Data availability

The seismic and well data used in creating the seismic surfaces in this study are available from the DISKOS database of the Norwegian Petroleum Directorate (<https://www.npd.no/en/diskos/>) and from TGS.

Received: 26 September 2022; Accepted: 16 June 2023;

Published online: 29 June 2023

References

1. Straume, E. O., Gaina, C., Medvedev, S. & Nisancioglu, K. H. Global Cenozoic paleobathymetry with a focus on the Northern Hemisphere oceanic gateways. *Gondwana Res.* **86**, 126–143 (2020).
2. Rossi, V. M., Longhitano, S. G., Olariu, C. & Chiocci, F. L. Straits and Seaways: end members within the continuous spectrum of the dynamic connection between basins. *Geol. Soc.* **523**, 2022–2159 (2023).
3. Hutchinson, D. K. et al. Arctic closure as a trigger for Atlantic overturning at the Eocene–Oligocene transition. *Nat. Commun.* **10**, 1–9 (2019).
4. Jakobsson, M. et al. The early Miocene onset of a ventilated circulation regime in the Arctic Ocean. *Nature* **447**, 986–990 (2007).

5. GEBCO. *GEBCO_2022 Grid*. <https://doi.org/10.5285/e0f0bb80-ab44-2739-e053-6c86abc0289c> (2022).
6. Norgaard-Pedersen, N. et al. Arctic Ocean during the Last Glacial Maximum: Atlantic and polar domains of surface water mass distribution and ice cover. *Paleoceanography* **18**, <https://doi.org/10.1029/2002PA000781> (2003).
7. Ehlers, B.-M. & Jokat, W. Paleo-bathymetry of the northern North Atlantic and consequences for the opening of the Fram Strait. *Marine Geophys. Res.* **34**, 25–43 (2013).
8. Knies, J. & Gaina, C. Middle Miocene ice sheet expansion in the Arctic: views from the Barents Sea. *Geochem. Geophys. Geosyst.* **9**, <https://doi.org/10.1029/2007GC001824> (2008).
9. Hossain, A., Knorr, G., Jokat, W. & Lohmann, G. Opening of the Fram Strait led to the establishment of a modern-like three-layer stratification in the Arctic Ocean during the Miocene. *Arktos* **7**, 1–12 (2021).
10. Engen, Ø., Faleide, J. I. & Dyrreng, T. K. Opening of the Fram Strait gateway: a review of plate tectonic constraints. *Tectonophysics* **450**, 51–69 (2008).
11. Kristoffersen, Y. in *Geological History of the Polar Oceans: Arctic Versus Antarctic* 63–76 (Springer, 1990).
12. Lasabuda, A. P. et al. Cenozoic uplift and erosion of the Norwegian Barents Shelf—a review. *Earth-Science Reviews* **217**, 103609 (2021).
13. Faleide, J. I., Bjørlykke, K. & Gabrielsen, R. H. in *Petroleum Geoscience: From Sedimentary Environments to Rock Physics* (ed K. Bjørlykke) 603–637. (Springer Nature, 2015).
14. Lasabuda, A., Laberg, J. S., Knutsen, S.-M. & Høgseth, G. Early to middle Cenozoic paleoenvironment and erosion estimates of the southwestern Barents Sea: Insights from a regional mass-balance approach. *Mar. Pet. Geol.* **96**, 501–521 (2018).
15. Butt, F. A., Drange, H., Elverhøi, A., Otterå, O. H. & Solheim, A. Modelling Late Cenozoic isostatic elevation changes in the Barents Sea and their implications for oceanic and climatic regimes: preliminary results. *Quat. Sci. Rev.* **21**, 1643–1660 (2002).
16. Zieba, K. J., Omosanya, K. O. & Knies, J. A flexural isostasy model for the Pleistocene evolution of the Barents Sea bathymetry. *Norw. J. Geol.* **97**, 1–19 (2017).
17. Medvedev, S., Faleide, J. I. & Hartz, E. H. Cenozoic reshaping of the Barents-Kara Shelf: Influence of erosion, sedimentation, and glaciation. *Geomorphology* **420**, 108500 (2023).
18. Haq, B. U., Hardenbol, J. & Vail, P. R. Chronology of fluctuating sea levels since the Triassic. *Science* **235**, 1156–1167 (1987).
19. Miller, K. G. et al. Cenozoic sea-level and cryospheric evolution from deep-sea geochemical and continental margin records. *Sci. Adv.* **6**, eaaz1346 (2020).
20. Ryseth, A. et al. Cenozoic stratigraphy and evolution of the Sørvestsnaget Basin, southwestern Barents Sea. *Norw. J. Geol.* **83**, 107–130 (2003).
21. Eidvin, T. & Riis, F. Nye dateringer av de tre vestligste borehullene i Barentshavet. Resultater og konsekvenser for den tertiære hevingen. *Nor. Pet. Dir. Contr.* **27**, 1–62 (1989).
22. Nikishin, A. M. et al. Arctic Ocean Mega Project: Paper 3-Mesozoic to Cenozoic geological evolution. *Earth Sci. Rev.* **217**, 103034 (2021).
23. Sømme, T., Doré, A., Lundin, E. & Tørudbakken, B. J. A. B. Triassic–Paleogene paleogeography of the Arctic: implications for sediment routing and basin fill. *AAPG Bull.* **102**, 2481–2517 (2018).
24. Dimakis, P., Braathen, B. I., Faleide, J. I., Elverhøi, A. & Gudlaugsson, S. T. Cenozoic erosion and the preglacial uplift of the Svalbard–Barents Sea region. *Tectonophysics* **300**, 311–327 (1998).
25. Smedsrud, L. H., Ingvaldsen, R., Nilsen, J. & Skagseth, Ø. Heat in the Barents Sea: transport, storage, and surface fluxes. *Ocean Sci.* **6**, 219–234 (2010).
26. Piepjohn, K., von Gosen, W. & Tessensohn, F. The Eureka deformation in the Arctic: an outline. *J. Geol. Soc.* **173**, 1007–1024 (2016).
27. Eiken, O. & Hinz, K. Contourites in the Fram Strait. *Sediment. Geol.* **82**, 15–32 (1993).
28. Rydningen, T. A. et al. An early Neogene–Early quaternary contourite drift system on the SW Barents Sea continental margin, Norwegian Arctic. *Geochem. Geophys. Geosyst.* **21**, e2020GC009142 (2020).
29. Bjordal-Olsen, S., Rydningen, T. A., Laberg, J. S., Lasabuda, A. P. & Knutsen, S.-M. Contrasting Neogene–Quaternary continental margin evolution offshore mid-north Norway: Implications for source-to-sink systems. *Mar. Geol.* **456**, 106974 (2022).
30. Hohbein, M. & Cartwright, J. 3D seismic analysis of the West Shetland Drift system: Implications for Late Neogene palaeoceanography of the NE Atlantic. *Mar. Geol.* **230**, 1–20 (2006).
31. Vorren, T. O., Richardsen, G., Knutsen, S.-M. & Henriksen, E. Cenozoic erosion and sedimentation in the western Barents Sea. *Mar. Pet. Geol.* **8**, 317–340 (1991).
32. Patton, H. et al. The extreme yet transient nature of glacial erosion. *Nat. Commun.* **13**, 1–14 (2022).
33. Faleide, J. I. et al. Late Cenozoic evolution of the western Barents Sea–Svalbard continental margin. *Global Planet. Change* **12**, 53–74 (1996).
34. Laberg, J. S., Andreassen, K., Knies, J., Vorren, T. O. & Winsborrow, M. Late Pliocene–Pleistocene development of the Barents Sea ice sheet. *Geology* **38**, 107–110 (2010).
35. Knies, J. et al. The Plio-Pleistocene glaciation of the Barents Sea–Svalbard region: a new model based on revised chronostratigraphy. *Quat. Sci. Rev.* **28**, 812–829 (2009).
36. Fiedler, A. & Faleide, J. I. Cenozoic sedimentation along the southwestern Barents Sea margin in relation to uplift and erosion of the shelf. *Global Planet. Change* **12**, 75–93 (1996).
37. Laberg, J. S., Andreassen, K. & Vorren, T. O. Late Cenozoic erosion of the high-latitude southwestern Barents Sea shelf revisited. *Geol. Soc. Am. Bull.* **124**, 77–88 (2012).
38. Hjelstuen, B. O. & Sejrup, H. P. Latitudinal variability in the Quaternary development of the Eurasian ice sheets—Evidence from the marine domain. *Geology* **49**, 346–351 (2021).
39. Lasabuda, A. et al. Late Cenozoic erosion estimates for the northern Barents Sea: Quantifying glacial sediment input to the Arctic Ocean. *Geochem. Geophys. Geosyst.* **19**, 4876–4903 (2018).
40. Lien, Ø. F., Hjelstuen, B. O., Zhang, X. & Sejrup, H. P. Late Plio-Pleistocene evolution of the Eurasian Ice Sheets inferred from sediment input along the NE Atlantic. *Quat. Sci. Rev.* **282**, 107433 (2022).
41. Alexandropoulos, N. et al. A continuous seismostratigraphic framework for the Western Svalbard–Barents Sea Margin over the last 2.7 Ma: Implications for the late Cenozoic Glacial history of the Svalbard–Barents Sea Ice Sheet. *Front. Earth Sci.* **9**, 656732 (2021).
42. Serov, P., Mattingdsdal, R., Winsborrow, M., Patton, H. & Andreassen, K. Widespread natural methane and oil leakage from sub-marine Arctic reservoirs. *Nat. Commun.* **14**, 1782 (2023).
43. Plaza-Faverola, A. et al. In *World Atlas of Submarine Gas Hydrates in Continental Margins* (Eds Mienert, J. et al.) 225–235 (Springer, 2022).
44. Henriksen, E. et al. Uplift and erosion of the greater Barents Sea: impact on prospectivity and petroleum systems. *Geol. Soc., London, Memo.* **35**, 271–281 (2011).
45. Lasabuda, A., Laberg, J. S., Knutsen, S.-M. & Safronova, P. Cenozoic tectonostratigraphy and pre-glacial erosion: a mass-balance study of the northwestern Barents Sea margin, Norwegian Arctic. *J. Geodyn.* **119**, 149–166 (2018).
46. Nyland, B., Jensen, L., Skagen, J., Skarpnes, O. & Vorren, T. in *Tectonic Modelling and Its Implication to Petroleum Geology* (Eds Larsen, R. M. et al.) 153–162 (Elsevier, 1992).
47. Doré, A. & Jensen, L. The impact of late Cenozoic uplift and erosion on hydrocarbon exploration: offshore Norway and some other uplifted basins. *Global Planet. Change* **12**, 415–436 (1996).
48. Riis, F. & Fjeldskaar, W. in *Structural and Tectonic Modelling and Its Application to Petroleum Geology* Vol. 1 (eds R. M. Larsen, H. Brekke, B. T. Larsen, & E. Taleraas) 163–185 (Norwegian Petroleum Society Special Publications, 1992).
49. Ohm, S. E., Karlsen, D. A. & Austin, T. Geochemically driven exploration models in uplifted areas: Examples from the Norwegian Barents Sea. *AAPG Bull.* **92**, 1191–1223 (2008).
50. Kuszniir, N. J., Roberts, A. M. & Morley, C. K. Forward and reverse modelling of rift basin formation. *Geol. Soc.* **80**, 33–56 (1995).
51. Roberts, A. M., Kuszniir, N. J., Yielding, G. & Styles, P. 2D flexural backstripping of extensional basins; the need for a sideways glance. *Pet. Geosci.* **4**, 327–338 (1998).
52. Klitzke, P., Faleide, J., Scheck-Wenderoth, M. & Sippel, J. A lithosphere-scale structural model of the Barents Sea and Kara Sea region. *Solid Earth* **6**, 153–172 (2015).
53. Faleide, J. I. et al. Tectonic implications of the lithospheric structure across the Barents and Kara shelves. *Geol. Soc.* **460**, 285–314 (2018).
54. Clark, S. et al. Southwest Barents Sea rift basin evolution: comparing results from backstripping and time-forward modelling. *Basin Res.* **26**, 550–566 (2014).
55. Gac, S., Hansford, P. A. & Faleide, J. I. Basin modelling of the SW Barents Sea. *Mar. Pet. Geol.* **95**, 167–187 (2018).
56. Eidvin, T., Goll, R. M., Grogan, P., Smelror, M. & Ulleberg, K. The Pleistocene to Middle Eocene stratigraphy and geological evolution of the western Barents Sea continental margin at well site 7316/5-1 (Bjørnøya West area). *Norsk Geol. Tidsskr.* **78**, 99–124 (1998).
57. Eidvin, T., Riis, F., Brekke, H. & Smelror, M. A revised lithostratigraphic scheme for the Eocene to Pleistocene succession on the Norwegian continental shelf. *Norw. J. Geol.* **1**, 1–132 (2022).
58. Knutsen, S.-M. & Vorren, T. O. Early Cenozoic sedimentation in the Hammerfest Basin. *Mar. Geol.* **101**, 31–48 (1991).
59. Gac, S., Minakov, A., Shephard, G. E., Faleide, J. I. & Planke, S. Deformation analysis in the Barents Sea in relation to Paleogene transpression along the Greenland–Eurasia Plate boundary. *Tectonics* **39**, e2020TC006172 (2020).

60. Smelror, M., Petrov, O., Larssen, G. B. & Werner, S. *Geological History of the Barents Sea*. Norges Geol. undersøkelse **1**, 1–135 (2009).
61. Saffronova, P. A., Henriksen, S., Andreassen, K., Laberg, J. S. & Vorren, T. O. Evolution of shelf-margin clinoforms and deep-water fans during the middle Eocene in Sorvestsnaget Basin. *AAPG Bull.* **98**, 515–544 (2014).
62. Eidvin, T., Riis, F., Rasmussen, E. & Rundberg, Y. Investigation of Oligocene to lower Pliocene deposits in the Nordic offshore area and onshore Denmark. *NPD Bull.* **10**, 62 (2013).
63. Rasmussen, E. S., Heilmann-Clausen, C., Waagstein, R. & Eidvin, T. The tertiary of Norden. *Episodes* **31**, 66 (2008).
64. Herold, N., Seton, M., Müller, R., You, Y. & Huber, M. Middle Miocene tectonic boundary conditions for use in climate models. *Geochem. Geophys. Geosyst.* **9**, 10 (2008).
65. Blakey, R. Paleotectonic and paleogeographic history of the Arctic region. *Atlantic Geol.* **57**, 7–39 (2021).
66. Sættem, J. et al. Cenozoic margin development and erosion of the Barents Sea: core evidence from southwest of Bjørnøya. *Mar. Geol.* **118**, 257–281 (1994).
67. Amantov, A. & Fjeldskaar, W. Meso-Cenozoic exhumation and relevant isostatic process: The Barents and Kara shelves. *J. Geodyn.* **118**, 118–139 (2018).
68. Rasmussen, E. & Fjeldskaar, W. Quantification of the Pliocene-Pleistocene erosion of the Barents Sea from present-day bathymetry. *Global Planet. Change* **12**, 119–133 (1996).
69. Poirier, A. & Hillaire-Marcel, C. Improved Os-isotope stratigraphy of the Arctic Ocean. *Geophys. Res. Lett.* **38**, 14 (2011).
70. Brinkhuis, H. et al. Episodic fresh surface waters in the Eocene Arctic Ocean. *Nature* **441**, 606–609 (2006).
71. Bergh, S. G., Braathen, A. & Andresen, A. Interaction of basement-involved and thin-skinned tectonism in the Tertiary fold-thrust belt of central Spitsbergen, Svalbard. *AAPG Bull.* **81**, 637–661 (1997).
72. Iakovleva, A. I., Brinkhuis, H. & Cavagnetto, C. Late Palaeocene–Early Eocene dinoflagellate cysts from the Turgay Strait, Kazakhstan; correlations across ancient seaways. *Palaeogeogr. Palaeoclimatol. Palaeoecol.* **172**, 243–268 (2001).
73. Poblete, F. et al. Towards interactive global paleogeographic maps, new reconstructions at 60, 40 and 20 Ma. *Earth Sci. Rev.* **214**, 103508 (2021).
74. Straume, E. O., Nummelin, A., Gaina, C. & Nisancioglu, K. H. Climate transition at the Eocene–Oligocene influenced by bathymetric changes to the Atlantic–Arctic oceanic gateways. *Proc. Natl. Acad. Sci. USA* **119**, e2115346119 (2022).
75. Hutchinson, D. K. et al. The Eocene–Oligocene transition: a review of marine and terrestrial proxy data, models and model–data comparisons. *Clim. Past* **17**, 269–315 (2021).
76. Blaich, O., Tsikalas, F. & Faleide, J. New insights into the tectono-stratigraphic evolution of the southern Stappen High and its transition to Bjørnøya Basin, SW Barents Sea. *Mar. Pet. Geol.* **85**, 89–105 (2017).
77. Rebesco, M., Hernández-Molina, F. J., Van Rooij, D. & Wählin, A. Contourites and associated sediments controlled by deep-water circulation processes: state-of-the-art and future considerations. *Mar. Geol.* **352**, 111–154 (2014).
78. Rodrigues, S. et al. A new classification system for mixed (turbidite-contourite) depositional systems: examples, conceptual models and diagnostic criteria for modern and ancient records. *Earth Sci. Rev.* **230**, 104030 (2022).
79. Sclater, J. G. & Christie, P. A. Continental stretching: an explanation of the post-Mid-Cretaceous subsidence of the central North Sea Basin. *J. Geophys. Res. Solid Earth* **85**, 3711–3739 (1980).
80. McKenzie, D. Some remarks on the development of sedimentary basins. *Earth Planet. Sci. Lett.* **40**, 25–32 (1978).
81. Watts, A. B. *Isostasy and Flexure of the Lithosphere* (Cambridge University Press, 2001).
82. Faleide, J. I. et al. Structure and evolution of the continental margin off Norway and the Barents Sea. *Episodes* **31**, 82–91 (2008).
83. Fjeldskaar, W. & Amantov, A. Effects of glaciations on sedimentary basins. *J. Geodyn.* **118**, 66–81 (2018).
84. Skogseid, J. et al. NE Atlantic continental rifting and volcanic margin formation. *Geol. Soc. Lett.* **167**, 295–326 (2000).
85. Theissen, S. & Rüpke, L. Feedbacks of sedimentation on crustal heat flow: New insights from the Vøring Basin, Norwegian Sea. *Basin Res.* **22**, 976–990 (2010).
86. Abdelmalak, M. M. et al. Quantification and restoration of the pre-drift extension across the NE Atlantic conjugate margins during the mid-Permian–early Cenozoic multi-rifting phases. *Tectonics* **42**, 1 (2023).
87. Baldwin, B. & Butler, C. O. Compaction curves. *AAPG Bull.* **69**, 622–626 (1985).
88. Dickinson, G. Geological aspects of abnormal reservoir pressures in Gulf Coast Louisiana. *AAPG Bull.* **37**, 410–432 (1953).
89. Athy, L. F. Density, porosity, and compaction of sedimentary rocks. *AAPG Bull.* **14**, 1–24 (1930).
90. Ellis, D. Formation porosity estimation from density logs. *Petrophysics* **44**, 306–316 (2003).
91. Jones, S. M. et al. A joint geochemical–geophysical record of time-dependent mantle convection south of Iceland. *Earth Planet. Sci. Lett.* **386**, 86–97 (2014).
92. Cramer, F., Shephard, G. E. & Heron, P. J. The misuse of colour in science communication. *Nat. Commun.* **11**, 1–10 (2020).

Acknowledgements

This research was funded by the *Akademia* programme (Equinor & UiT The Arctic University of Norway). Financial support from the Research Council of Norway is acknowledged to the Research Centre for Arctic Petroleum Exploration (ARCEX) and “The dynamics of polar confined basins—the Eurasia Basin from breakup in greenhouse to present in icehouse conditions” (DYPOLE) projects (grants no. 228107 and 325984), and through its Centres of Excellence funding scheme (grants no. 223259 and 223272) for the Centre for Arctic Gas Hydrate, Environment and Climate (CAGE) and Centre for Earth Evolution and Dynamics (CEED). We acknowledge educational software licenses of Petrel (Schlumberger) and 3D MOVE (Petroleum Experts Ltd.) for the Department of Geosciences, UiT The Arctic University of Norway and the Department of Earth Sciences, Royal Holloway University of London. Perceptually uniform colour ramps of Cramer et al.⁹² were used to prevent visual distortion. We thank the reviewers, including Davide Gamboa and Morten Smelror, for their detailed and constructive comments.

Author contributions

A.P.E.L. performed the numerical modelling, wrote the initial manuscript and prepared the figures and tables. A.H. and J.S.L. conceived the study. M.M.A. prepared the beta factor maps. B.K. converted the seismic surfaces from time to depth. J.I.F., H.P., T.A.R. and all authors contributed to editing and reviewing the manuscript.

Funding

Open access funding provided by UiT The Arctic University of Norway (incl University Hospital of North Norway).

Competing interests

The authors declare no competing interests.

Additional information

Supplementary information The online version contains supplementary material available at <https://doi.org/10.1038/s43247-023-00899-y>.

Correspondence and requests for materials should be addressed to Amando P. E. Lasabuda.

Peer review information *Communications Earth & Environment* thanks Davide Gamboa, Morten Smelror and the other, anonymous, reviewer(s) for their contribution to the peer review of this work. Primary Handling Editors: João Duarte and Joe Aslin. A peer review file is available.

Reprints and permission information is available at <http://www.nature.com/reprints>

Publisher's note Springer Nature remains neutral with regard to jurisdictional claims in published maps and institutional affiliations.



Open Access This article is licensed under a Creative Commons Attribution 4.0 International License, which permits use, sharing, adaptation, distribution and reproduction in any medium or format, as long as you give appropriate credit to the original author(s) and the source, provide a link to the Creative Commons license, and indicate if changes were made. The images or other third party material in this article are included in the article's Creative Commons license, unless indicated otherwise in a credit line to the material. If material is not included in the article's Creative Commons license and your intended use is not permitted by statutory regulation or exceeds the permitted use, you will need to obtain permission directly from the copyright holder. To view a copy of this license, visit <http://creativecommons.org/licenses/by/4.0/>.

© The Author(s) 2023